

Satellite Imaging and Characterization with Optical Interferometry

Anders M. Jorgensen^a, Eric J. Bakker, G. C. Loos^a, D. Westpfahl^a, J. T. Armstrong^b,
R. L. Hindsley^b, H. R. Schmitt^b, S. R. Restaino^b

^aNew Mexico Institute of Mining and Technology, Socorro, NM, USA

^bNaval Research Laboratory, Washington, DC, USA

ABSTRACT

In this paper we discuss the possibility of imaging geostationary satellites with optical interferometers. Geostationary satellites are generally too large to image in a resolved way with conventional single-dish telescopes. However, optical interferometers can be used to increase the angular resolution. Interferometric imaging of satellites is different from the imaging of stars where Earth-rotation synthesis can be employed. Instead it is necessary to combine an interferometer with many baselines with wavelength synthesis, and that produces the ability to make crude images. From the point of view of existing interferometers most geostationary satellites are large targets. That reduces the observed visibility which can make fringe-tracking difficult. We find that a larger aperture (such as are planned for the MROI) under ideal conditions, and assuming the satellite is a perfect diffuse reflector, can track fringes on many satellites in the typical range of satellite brightnesses, but that any small deviations, such as non-ideal seeing or imperfect reflection from the satellite, can significantly narrow the number of targets. The equinox glint can help. However, using the equinox glint to track fringes will hurt imaging performance, requiring a much larger increase of the already long integration time. We conclude that, although more detailed modeling is required, imaging geostationary satellites with interferometers may be feasible if large apertures are used, an exceptionally good site is used or the telescopes are equipped with effective adaptive optics, and coherent integration techniques, large (10) number of telescopes, and wavelength synthesis are made use of.

1. INTRODUCTION

The US Department of Defense (DOD) has established and operates a worldwide network of ground and space based telescopes and other sensors in support of its Space Situational Awareness (SSA) program. SSA provides a continuing threat assessment of a large number of space vehicles incorporating launch detection, initial determination of orbital elements, catalog maintenance of orbits, and determination of operational status. The satellite components of the catalog are commonly separated into two broad categories; satellites with orbits on the order of 1000 km or less being categorized as low earth orbit (LEO) while those in the highest orbits are usually represented by geostationary (GEO) satellites operating at altitudes of approximately 36,000 km. GEO satellites are typically very large, very high value (> \$10⁹!) satellites providing essential military and civilian communication services (such as satellite TV signal and other communications). This paper will examine the technical issues involved in obtaining resolved images of GEO satellites from the ground through the use of optical interferometry. The capability of large ground based telescopes to obtain high resolution images of sources on the sky has historically been limited by the blurring effects of turbulence in the Earth's atmosphere. In more recent years the development and im-

plementation of adaptive optical system technologies, often together with advanced image processing techniques, has enabled these same telescopes to routinely image at or near their diffraction limited performance. However if even higher resolution imagery is needed it then becomes necessary to find a way or ways to further increase the theoretical resolving power of our telescope systems. In so far as various cost, engineering, and other practical issues restrict the maximum diameter of current generation telescopes to the order of 8 to 10 meters we must look elsewhere to find how this resolution might be achieved. In this paper we consider the application of distributed aperture optical interferometry as an aperture synthesis technique for obtaining resolved images of geostationary satellites. The principle advantage of any interferometer designed to image on the sky is that, at least in principle, the achievable resolution is determined by the separation(s) of the interferometers sub apertures or component telescopes, i.e. $\frac{\lambda}{B}$ where B is the telescope separation, rather than by $\frac{\lambda}{D}$ where D is any component telescopes diameter. Using this technique it becomes possible to achieve resolutions significantly smaller than the diffraction limit associated with any large ground based telescope no matter its mirror diameter. If we are to consider the possibility of imaging geostationary satellites, the requirement

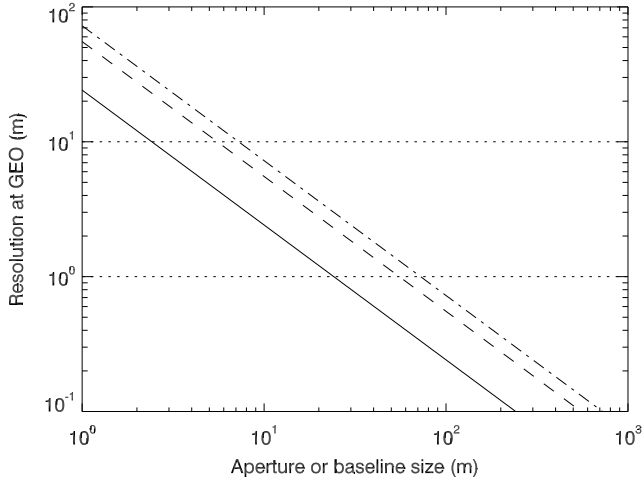


Figure 1. Resolution at geostationary orbit of a ground-based telescope as a function of baseline length (or equivalently aperture diameter for a single telescope) for three different astronomical bands, V (solid), J (dashed), and H (dash-dotted), at wavelengths of $0.55 \mu\text{m}$, $1.2 \mu\text{m}$, and $1.65 \mu\text{m}$, respectively.

for an optical interferometer with extended baselines becomes immediately apparent. The resolution, equivalent to the smallest resolvable feature on orbit, can be shown to be $1.22 \frac{R\lambda}{B}$. Figure 1 shows the resolution at geostationary orbit as a function of baseline length (or equivalently aperture diameter for a single telescope) for a ground-based observatory at three different astronomical bands, V, J, and H, at wavelengths of $0.55 \mu\text{m}$, $1.2 \mu\text{m}$, and $1.65 \mu\text{m}$, respectively.

It is apparent that resolving a feature as small as 0.1 m even at J band will require baseline telescope separations of 100s of meters. Unfortunately, it will prove to be very difficult to acquire and track fringes on faint geostationary satellites as will be discussed later in this paper. Nevertheless, even poorly resolved images, i.e. with a resolution of 1 to 2 m, of geostationary satellites will still yield valuable information concerning these systems' orientation and operational status and lend support to the viability of this technique for geostationary SSA. There has already been some useful work done in the area of satellite imaging by interferometry and we must recognize that here. The Navy Prototype Optical Interferometer¹ (NPOI) has demonstrated the phasing of an optical baseline on a GEO source using a specular reflection of sunlight from the source.²⁻⁵ Figure 2 shows these data and a fit of a two-component model, a brighter more compact component (diameter approximately 1 m), and a fainter more extended component (diameter approximately 7 m). These specular reflections or glints are typically many visual magnitudes brighter than the always present diffuse reflected

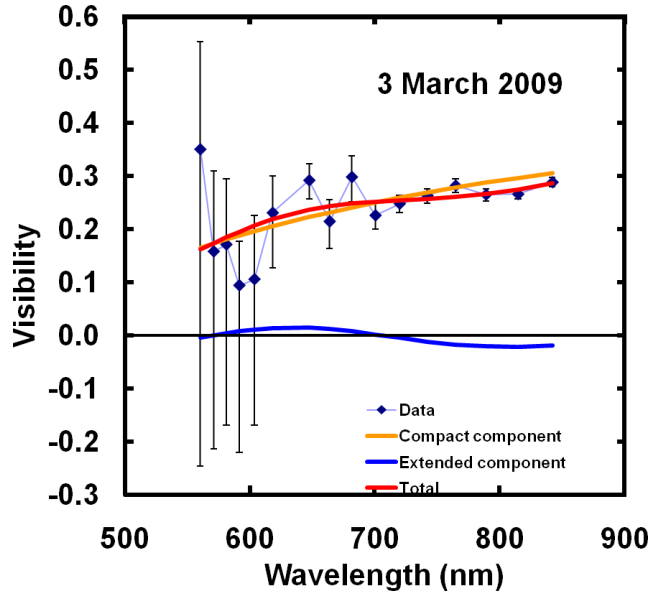


Figure 2. Observation of a glint on a geostationary satellite. The visibility is consistent with a two-component source, a compact source of diameter approximately 1 m and a extended source of diameter approximately 7 m.

component but limited in their angular projection and temporal duration. The small angular size and large brightness makes it easier to track fringes on glints than on the whole satellite. But the short duration and (paradoxically) large brightness make it more difficult to produce images, as we will see later in this paper. The Geo Light Imaging National Testbed⁶ (GLINT) is an imaging concept in which the geostationary satellite is flood illuminated by 3 lasers simultaneously. Two of these lasers are tagged with a frequency offset such the satellite is scanned in 2 dimensions by the fringe pattern formed by the laser irradiance at the satellite. The resulting scan modulation generates a closure phase which can be read by a simple photo detector on the ground. The GLINT concept did not proceed to system level testing.

There are several issues which must be considered for geostationary satellite imaging with an interferometer. Firstly, their sizes, shapes, and spectral characteristics should be understood and used as input to the rest of the derivations. This is discussed in section 2. Secondly, it should be possible to obtain a sufficient number of image elements with a reasonable number of baselines. The capabilities of different interferometers is discussed in section 3, and some examples of image reconstruction are shown in section 4. Thirdly, it should be possible to track fringes on the relatively faint and relatively large satellites. Fringe-tracking SNR is dis-

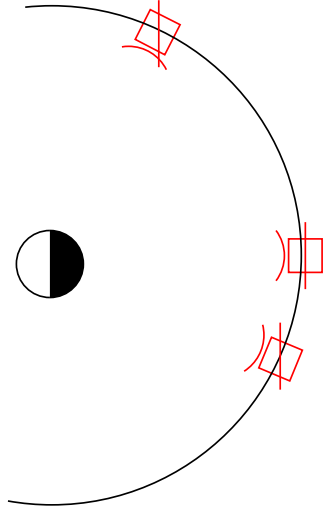


Figure 3. Both the actual and apparent shapes of geostationary satellites change as they orbit around the Earth. There is a actual shape change because the antennas remain pointed in the direction of the Earth while the solar panels remain pointed in the direction of the sun. There is also an apparent change in shape which is due to the changing sun-angle and thus changing illumination as the satellite progresses in its orbit.

cussed in section 5. Finally, it should be possible to obtain enough photons to obtain sufficiently good SNR to produce images. Imaging SNR is discussed in section 6. In section 7 we discuss the results and in section 8 we offer some conclusions and suggestions for future work.

2. CHARACTERISTICS OF SATELLITES

Geostationary satellites are relatively large for interferometric observations, but relatively small for observing with most conventional telescopes. A typical geostationary satellite has a body diameter of 2 to 10 m, antennas and solar panel widths of similar size, and solar panel lengths anywhere from 10 to 100 m. Because the satellite follows the rotation of the Earth while the solar panels remain pointed toward the sun and antennas toward the Earth, the satellite changes shape over time. Additionally, because the sun-angle changes with time the satellite also appears to change shape, as seen from the Earth, due to changes in illumination. Figure 3

Satellites are also faint. Figure 4 is a distribution of visual magnitudes of satellites obtained from.⁷ The majority of satellites have visual brightnesses between 12th and 16th magnitude.⁷ measured the colors of several different satellites, which we have adapted in Table 1. This table shows some consistent colors across all satellites. We use this to estimate the brightnesses in different bands. From this table we estimate, $V - I = 1.13 \pm$

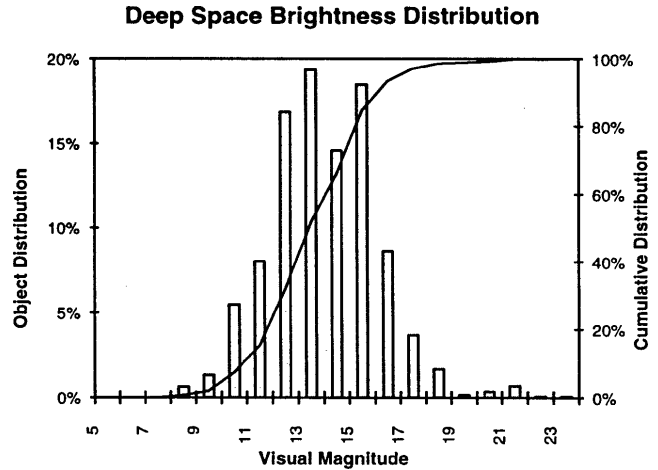


Figure 4. Histogram of visual magnitudes of satellites obtained from.⁷

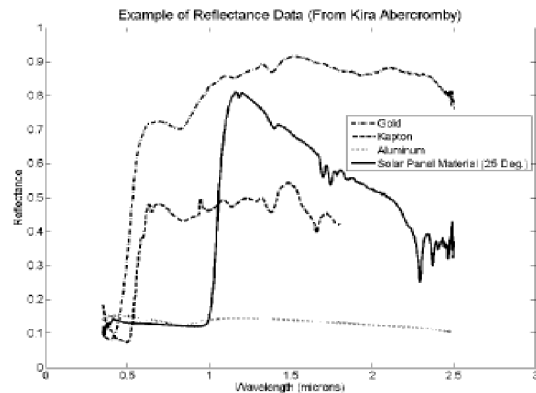


Figure 1 - Reflectances for Some of the Most Common Materials Used in GEOs

Figure 5. Reflectances of several common materials used in satellites, as a function of wavelength, from.⁸

0.16, $V - J = 2.78 \pm 0.41$, $V - H = 3.28 \pm 0.44$. Thus we expect the geostationary satellites to be roughly in the ranges of 10th to 14th magnitude in I, 9th to 13th in J, and 8th to 13th in H.

Part of these brightness differences are the result of the solar spectrum, and part of them are the result of different reflective characteristics of the materials which the satellites are made of. Figure 5 shows the reflectance of several common materials used in satellites, from.⁸ Two common materials are gold foil, which often covers a large fraction of the body for thermal control, and another is solar panels. Gold has a relatively large reflectance across much of the useful spectral range from $0.5 \mu\text{m}$ to $2.5 \mu\text{m}$, with some structure evident. Solar panels have, not surprisingly, very

Bus Type	Name	B	V	R	I	J	H
Hughes 601	AMSC 1	12.1	11.3	10.8	10.3	8.9	8.6
	DBS 1	12.8	12.0	11.5	11.0	8.6	8.2
	DBS 2	12.6	11.7	11.2	10.7	8.5	8.0
	DBS 3	12.5	11.8	11.3	10.7	8.8	8.3
	Solidaridad 1	12.5	11.7	11.1	10.6	8.7	8.1
	Solidaridad 2	12.2	11.4	10.9	10.4	8.3	7.6
GE Satcom 5000	AnikE 1	11.4	10.8	10.3	9.7	8.5	8.0
	AnikE 2	11.7	11.1	10.5	9.9	8.4	8.0
LMAS 3000	Gstar 4	14.1	13.4	12.8	12.1	11.0	10.4
	Spacenet 4	14.1	13.1	12.4	11.6	10.8	10.3

Table 1. Magnitudes of several different satellite buses, adapted from.⁷

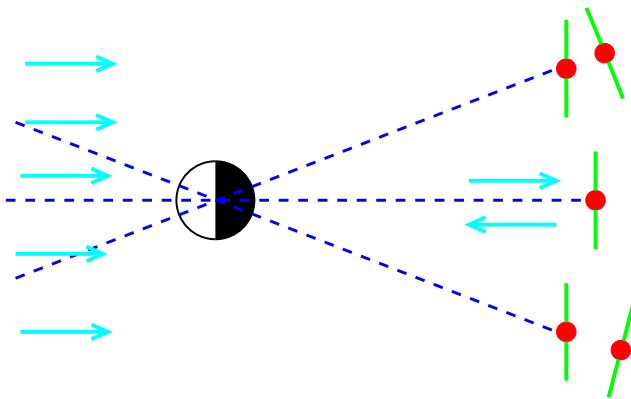


Figure 6. This figure illustrates the geometry between the satellites, the Sun, and the Earth. The horizontal line represents the equatorial plane along the noon-midnight meridian during equinoxes, whereas the other two dashed lines represent the equatorial plane during solstices. It can be seen that regardless of which of two standard orientations the solar panels take, it is only during equinoxes that there is the possibility of specular reflection, and only while the satellite is near the midnight meridian.

low reflectance at visible wavelength, and moderate reflectance at other wavelengths. It is important to distinguish between specular reflection, which is reflection from a flat mirror-like surface, and diffuse reflection which is reflection from a rough surface, and usually far less directional. Reflection off of most surfaces typically contain some specular components and some diffuse components.

As mentioned earlier, the real and/or apparent shape of the satellites changes as it orbits the Earth. During certain times of the year, for a few days around the March and September equinoxes, there is the possibility of specular reflection from the satellite solar panels as the satellite crosses the midnight meridian with the solar panels pointing at the sun. Figure 6 illustrates

this process. The dashed curves represent the equatorial plane, in which the satellite orbits, during December and June solstices for the tilted planes, and during equinoxes for the horizontal planes. The satellites are also sketched. Only near equinoxes is there a possibility of specular reflection off of a satellite, and only as the satellite transits the midnight meridian above the observatory. During these equinox passes the satellites can brighten by many orders of magnitude, including being visible to the unaided eye in some circumstances. During glints some satellites brighten sufficiently to be observable by the NPOI.

3. CAPABILITIES OF INTERFEROMETERS

There are 4 optical interferometers in operations in the US:

- Naval Prototype Optical Interferometer (NPOI)
- Center for High Resolution Astronomy (CHARA)
- Infrared Spatial Interferometer (ISI)
- Keck interferometer

There are 2 facilities which are in the construction phase

- Magdalena Ridge Observatory Interferometer (MROI)
- Large Binocular Observatory (LBO)

There are two facilities operating in other parts of the world

- Very Large Telescope Interferometer (VLTI)
- Sydney University Stellar Interferometer (SUSI)

In this paper we focus on the NPOI and the MROI as examples. The reason for that is that they both have or will have the capability to observe fringes on very short baselines, which we will see becomes important. Both these projects are funded by the Navy. NPOI has six telescopes each with a diameter of 12 cm. The minimum and maximum baselines are currently 5.5 m and 79 m (expansion to approximately 400 m will begin soon). The operating wavelength is the visible regime, 450 nm-850 nm. NPOI has been operational since 1994. MROI, which is planning for first light in December 2011, is designed to have up to 10 fully transportable telescopes each with a diameter of 1.4 m. The minimum baseline is planned to be 7.5 m and the longest baseline is 350 m. The operating wavelength will be from 600 nm to 2400 nm (R, I, J, H, and K bands). We should mention that while we refer to the NPOI and MROI in this paper they are simply intended as examples of interferometers with small and large apertures. For each we assumed a system V^2 of 0.3, throughputs of 5% for NPOI and 13% for MROI, and collecting areas as indicated by the diameters above.

4. IMAGE RECONSTRUCTION

4.1. How does interferometric imaging works?

If one takes the Fourier Transform of an image, this give a map in the UV-plane. An interferometer measures discrete points in the UV-plane. To make an image, the UV-plane is Fourier transformed back to the image plane. The difficulty with interferometers is that the UV-plane is only sampled at specific points (corresponding with a specific baseline) and that therefore the UV-plane is only sparsely filled by data. The information is incomplete. The Fourier Transform back to the image plane lacks therefore information to make a full image. The next, or combined, step is to apply an image reconstruction algorithms to improve the quality. Several techniques have been applied in the past for optical and radio interferometer. This includes clean, maximum-entropy and a few more. An overview can be found in Cotton et al. 2008.¹⁰

4.2. No earth rotation synthesis

For any snapshot image, on a single baseline, a single UV-point is sampled. The projected baseline on the sky is fixed. As the earth rotates around its axis (24 hour

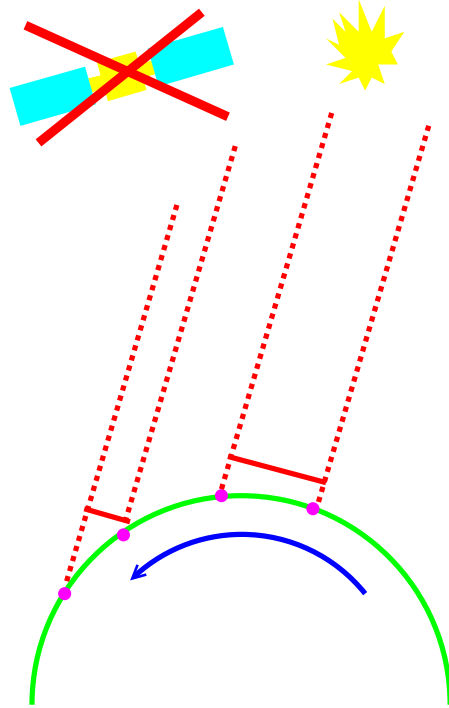


Figure 7. While Earth rotation synthesis can be used to increase the effective number of baselines for stellar observations it cannot be used to do the same for geostationary satellites. This is because geostationary satellites rotate with the Earth, whereas stars are fixed in the sky, thus seeing a different projected baseline as the hour-angle changes.

cycle) the object seems to move on the sky. The objects are tracked with the telescopes and that results in a changing projection of the baseline on the sky, and hence in a different UV points being sampled. This is referred to as UV tracks. For a geostationary satellite, the position above the earth is largely fixed and earth rotation synthesis does not apply (Figure 7).

4.3. Use spectral information instead

Another approach to increase the UV-sampling is by using a range of wavelengths. The UV-sampling point is dependent on the separation between the two telescopes, and the wavelength. For example, one could measure in the visible (500 nm), H- and K-band simultaneously. We have studied this approach⁹ and to first order it seems viable. If more details are to be seen, than the image reconstruction becomes much more complicated as different part of the satellite will have different spectral characteristics. In this is the case, the image reconstruction is not only a 2-dimensional problem, but becomes three dimensional as each pixel of the image could have their own specific spectral characteristics. Suggested ways to deals with this is putting advanced

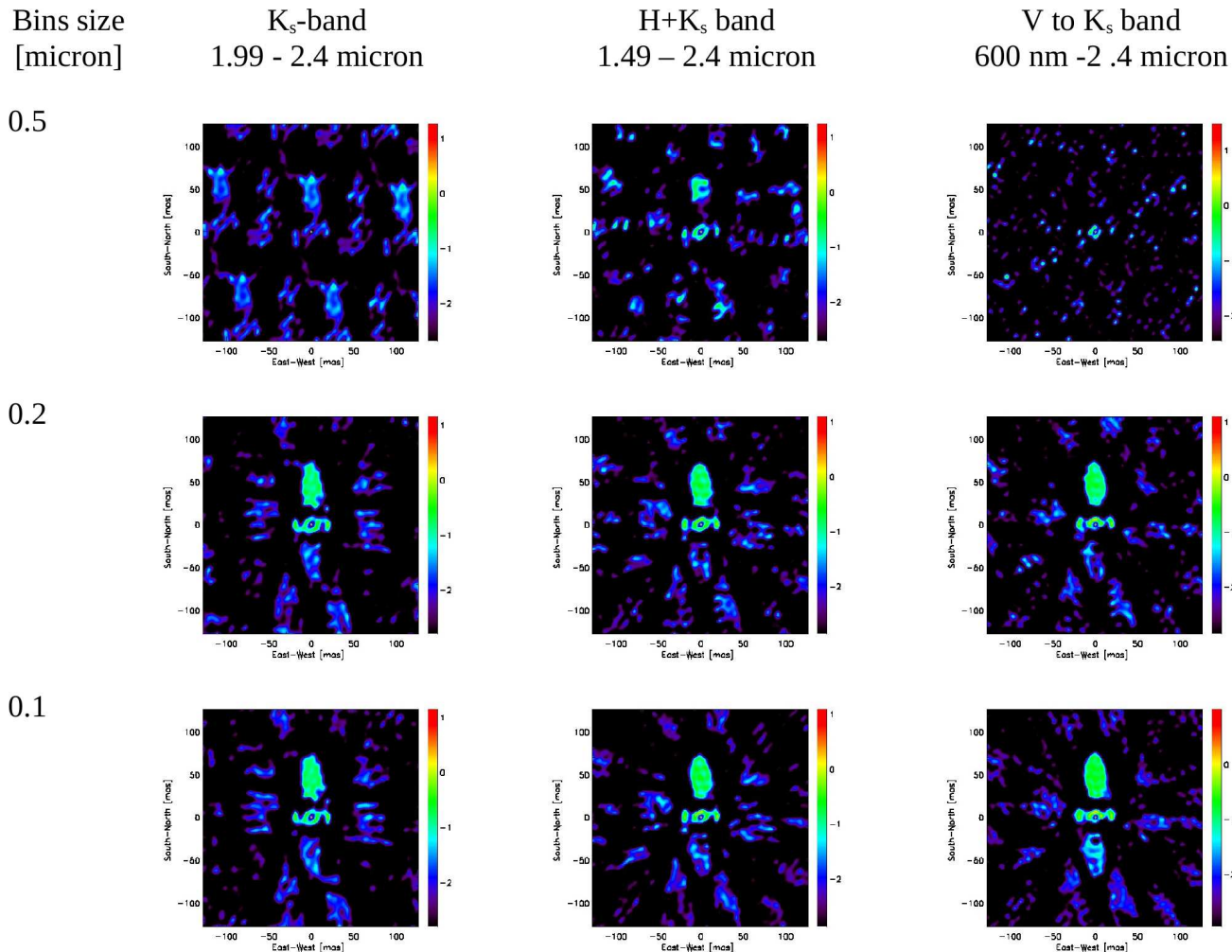


Figure 8. This figure taken from⁹ illustrates the use of wavelength synthesis in increasing the effective number of baselines used. The three columns correspond to three different wavelength ranges, and the three rows correspond to three different wavelength bin widths, such that the upper left image contains the smallest effective number of baselines and the lower right image contains the largest effective number of baselines.

knowledge in the image reconstruction algorithms. Either constraining certain geometric shapes, or spectra. If the target is known, and one knows what it suppose to look like, this information can be used to converge to a reconstructed image much quicker.

4.4. Simulations

Simulations were performed with software provided by the University of Cambridge, Cavendish group (UK). An observing strategy was computed with the program obstrat, visibilities were predicted for this strategy and the simplified geometric model of the target using the program bsfake. The output of these programs are the computed visibilities and closure phases. The image was reconstructed using the BSMEM software package that

uses a maximum entropy method to compute the reconstructed image.^{10,11} Figure 8 shows reconstructed satellite images for a varying number of baselines, taken from.⁹

5. FRINGE TRACKING SIGNAL-TO-NOISE

In order to observe geostationary satellites, or any target for that matter, it is necessary to track fringes. The ability to track fringes is determined by the fringe-tracking SNR, NV^2 , where N is the number of detected photons in one integration (approximately one atmospheric coherence time) and V is the visibility amplitude. In this paper we use a integration time of 2 ms at a

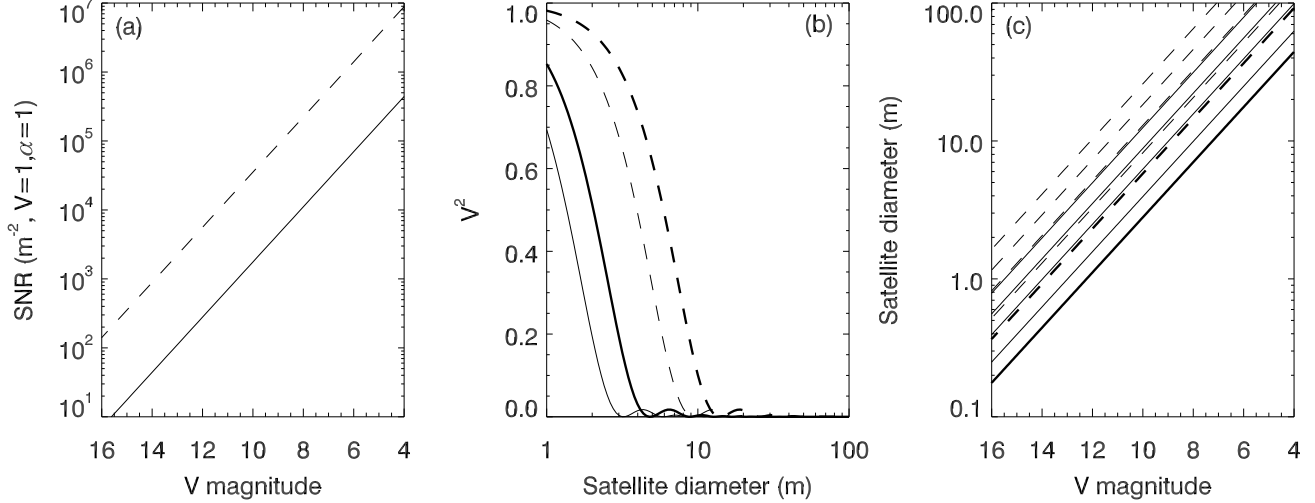


Figure 9. (a) Photon rate per m^2 of collecting area for a source of the indicated V magnitude in the V-band (solid) and H-band (dashed). It can also be interpreted as fringe tracking SNR for an unresolved source. (b) Squared visibility as a function of satellite diameter on the shortest baseline of NPOI (thick curves) and MROI (thin curves) in the V-band (solid) and H-band (dashed). (c) Relationship between satellite V magnitude and satellite diameter in the V-band (solid) and H-band (dashed), assuming a diffuse reflector of different albedo. The thick curves are for unity albedo and the other curves extending above and to the left are for albedos 0.5, 0.2, 0.1, and 0.05.

wavelength of 500 nm. For larger satellites the visibility on a given baseline tends to be smaller, but the satellites also tend to be brighter. For small satellites the visibility tends to be larger, but the satellite also tends to be fainter. In order to compute the balance of these effects we prepare three quantities, given in Figure 9. In panel a the photon rate per unit collecting area is computed in the V-band (solid) and H-band (dashed) as a function of the V magnitude of the satellite. In computing the H-band photon rate as a function of the V magnitude we use the approximate relationship between band magnitudes found in section 2. In panel b the squared visibility is plotted as a function of satellite diameter in the V-band (solid) and in the H-band (dashed), for the shortest NPOI baseline (thick lines) and the shortest MROI baseline (thin lines). NPOI and MROI are both distinguished by having the capability to observe on very short baselines, which allows very large targets, such as satellites, to be observed. The other interferometers in the list in section 3 each have much longer minimum baselines, which have very small visibilities, making it difficult to acquire fringes. In panel c we estimate the satellite diameter as a function of its visual magnitude using a spherical diffuse reflector model. The dashed lines are for H-band and the solid lines are for V-band. The thick lines are for unity albedo, and thus represent the minimum size of a spherical diffuse reflector. The other lines, from bottom to top, represent albedos of 0.5, 0.2, 0.1, and 0.05,

respectively. Because satellites are not diffuse reflectors and because they are not symmetric, it is possible that a satellite will be larger in one orientation than these estimates, or that it will be smaller in another orientation than these estimates. We will restrict ourselves to the spherically symmetric model here and leave more realistic satellite shapes for the future.

From Figure 9, panels a and b we can produce a contour plot of the fringe-tracking SNR as a function of satellite magnitude and satellite diameter. Such plots are shown in Figure 10. Panel a is for NPOI in H-band, panel b for MROI in H-band, panel c for NPOI in V-band, and panel d for MROI in V-band. In each plot the curved lines are contours of the fringe-tracking SNR, NV^2 . The solid curve represents $NV^2 = 10$, the dotted curves to the right of that higher SNR of 20 and 50, and the curves to the right of that smaller SNR of 5, 2, and 1. So, for example, a satellite with a V-band magnitude of 10 and a diameter of 8 m will have a fringe-tracking SNR of 10 when observed through the NPOI. The straight lines give the relationship between the satellite V-band magnitude and its diameter in the H- or V-band, depending on the panel. These relationships are taken from Figure 9c. The solid straight line is for unity reflectivity, and the dashed straight lines to the left of it are for smaller reflectivity: 0.5, 0.2, 0.1, and 0.05 going from right to left. The regions where fringe-tracking is possible are the regions to the left of the straight lines and to the right of the curves. We

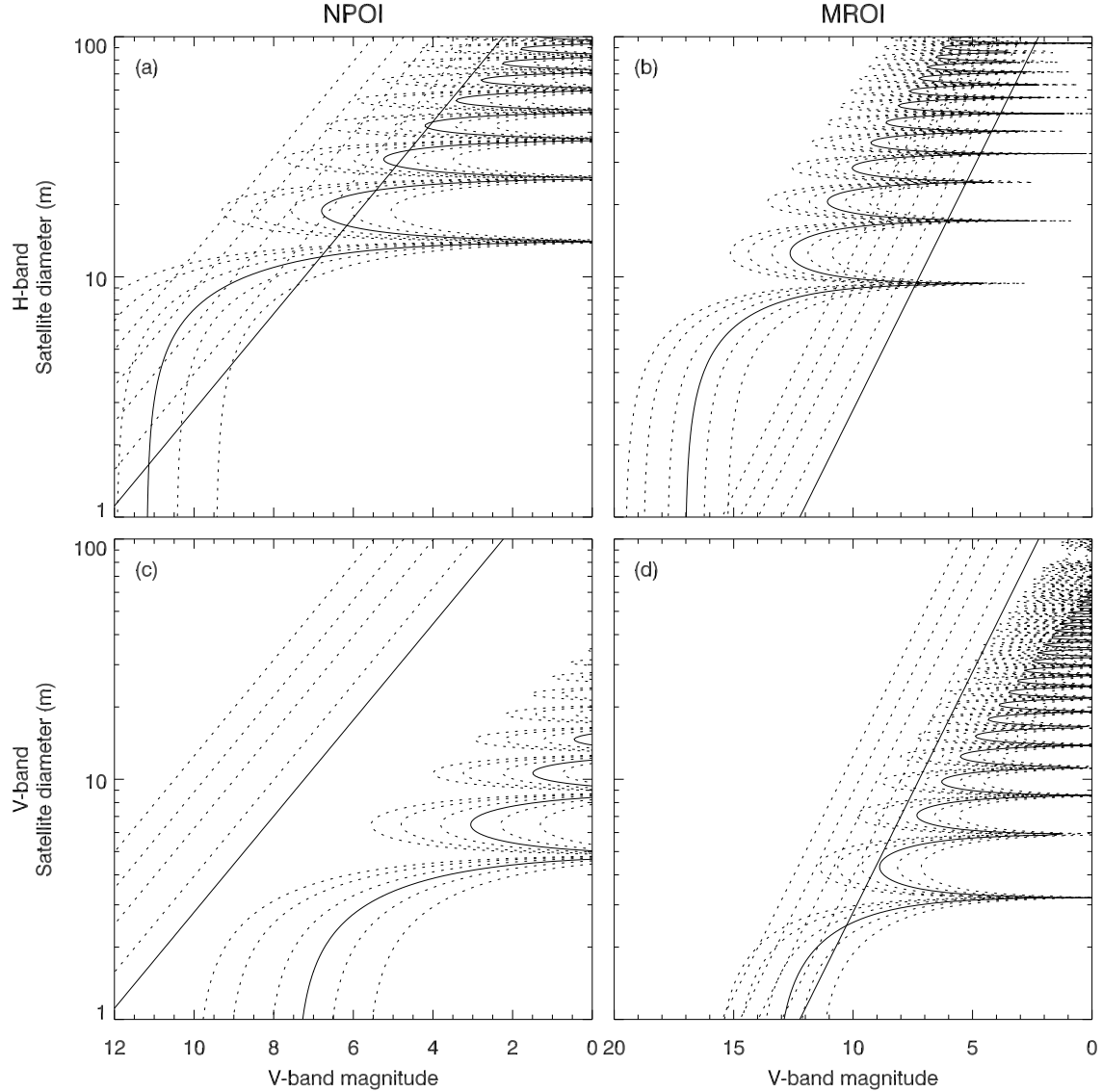


Figure 10. Contours of fringe-tracking SNR for (a) NPOI in H-band, (b) MROI in H-band, (c) NPOI in V-band, and (d) MROI in V-band, as a function of visible magnitude and satellite diameter (curved lines). The solid curved line represents a SNR of 10, the dotted ones to the right of the solid curved line SNR of 20 and 50, and the ones to the left SNR of 5, 2, and 1. The straight lines represent the relationship between satellite V-band magnitude and satellite diameter from Figure 9 in the band of the panel. The solid straight line is for a perfect diffuse reflector and the dashed curves to the left of it are for reflectivities of 0.5, 0.2, 0.1, and 0.05. The region in which fringe-tracking is possible is the area between a straight line and a curve.

can pick a minimum fringe-tracking SNR and a satellite reflectivity and map out the area. For example, in the V-band on the MROI (Figure 10d) it appears that MROI can just track on satellites with a V magnitude of around 12, if these satellites have a reflectivity of at least 0.5 and we assume a minimum SNR of 10 for fringe-tracking. A caveat to these numbers must be mentioned, and we will expand on this in the discussion section. For MROI the apertures are quite large com-

pared to the observed r_0 at the site, and these effects have not been taken into account. We therefore expect the numbers in Figure 10 to be overestimates of the performance. NPOI, with its smaller apertures, does not suffer from this problem, but, on the other hand, collects much fewer photons. Thus, fringe-tracking is out of the question in the visible at the NPOI. Another important point is that these numbers are not corrected for atmospheric extinction, which also contributes to

a optimistic estimate. Notwithstanding these complications, In the H-band there appears to be a much wider range of satellite magnitudes for which MROI can fringe-track. With the idealized models it appears that MROI may be able to track fringes on nearly all geostationary satellites visible to it. The NPOI should be able to track fringes on the few brightest satellite in the H-band.

This exercise illustrates the dual nature of the problem. In order to track fringes there needs to be sufficiently many photons per coherence time, and the visibility of the satellite needs to be sufficiently large. However, brighter satellites tend to be larger and thus have smaller visibilities, whereas more compact satellites with larger visibilities tend to produce fewer photons.

There is one exception to this, which was already discussed in section 2. When the satellite is glinting during a short period near equinox, the reflection is specular and thus very bright, and usually also compact. During those times the satellite can brighten to visual magnitudes glint spot diameters of only a couple meters or less. In this case both the MROI and the NPOI will be able to track fringes, very well in the H-band and reasonably well in the V-band.

6. IMAGING SNR

Because geostationary satellites are highly resolved objects the measured visibilities will tend to be small and a larger number of photons must be collected to obtain sufficient SNR on the visibilities to produce an image. In this paper we will assume that the complex visibilities have been obtained, for example via a coherent integration scheme similar to that described by.¹² In that case the SNR is \sqrt{NV} . We once again make use of the perfect diffuse reflector model and use that to compute the integration time for different resolutions. The results are in Figures 11-14. Figures 11 and 12 are for the case when fringes are tracked using a glint which is 10^3 times (7.5 magnitudes) brighter than the satellite, whereas figures 13 and 14 are for no fringe-tracking glint. Figures 11 and 13 are for V-band whereas Figures 12 and 14 are for H-band. If we look at Figure 11 we can see that in V-band, with a fringe-tracking glint, it takes 1 month, several days and one day, to obtain SNR=10 for V=16, 14, and 12, respectively on MROI, whereas the integration times at NPOI are many years, a few years, and one year, respectively. These are all unrealistically long integration times. From Figure 13 we see that these integration times are greatly reduced if there is no glint, to one hour, many minutes, and

a few minutes for MROI, and one month, a few days, and one day for NPOI. Without a glint it is possible to obtain images with 10 pixels across at the MROI, but integration times are still very long at NPOI. If we look at Figure 12 we can see that in H-band, with a fringe-tracking glint, it takes several days, one day, and several hours at the MROI for satellites of the same magnitudes as above, and several years, one year, and several months for NPOI. Except for the brightest satellites with MROI the integration times are unrealistically long. From Figure 14 we see that the integration times are again much smaller if there is no glint, several minutes, one minute, and seconds at MROI, and two days, several hours, and one hour at NPOI. These are very realistic integration times at MROI and doable integration times at the NPOI for the brighter satellites.

The reason why the presence of a glint increases the integration time is that while this increases the number of photons recorded it also effectively reduces the visibility of the rest of the satellite which we are trying to image. The glint helps track fringes, but at the same time it blinds the instrument from seeing the rest of the satellite, thus requiring much longer integration times to be able to image the satellite through the very bright glint.

7. DISCUSSION

In the previous we have described the characteristics of satellites, and then imaging fidelity from a 10-element interferometer with varying levels of wavelength synthesis. We found that it is possible to make crude images of geostationary satellites with a 10-element interferometer such as the MROI. Next we considered fringe-tracking SNR. We considered a perfect spherical diffuse reflector as the satellite model. We found that under this scenario it is necessary to use large apertures and preferentially track fringes in the H-band. In that case, under ideal conditions it should be possible for a MROI-like interferometer to track fringes on a wide range of satellites in the V=12 to V=16 magnitude range. This range covers the majority of satellites. However, if we relax the assumptions some, the window can narrow substantially and it becomes less clear precisely how faint we can go. For example, if the satellite is better modeled as a diffuse reflect with less than perfect albedo, then the V magnitude is effectively increased (brightness decreased). If the seeing at the MROI site is less than that for which the telescopes are designed, then the telescopes will need to be stopped down, thus increasing the minimum brightness (decreasing the minimum magnitude). The latter

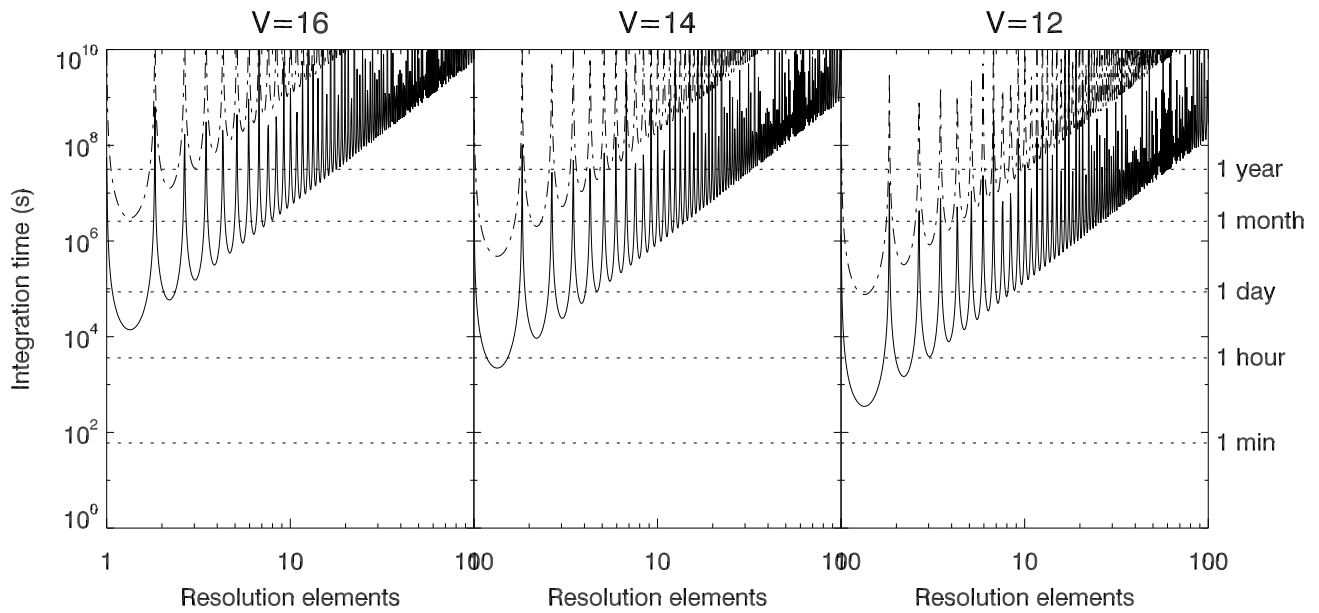


Figure 11. Integration time required to obtain imaging SNR of 10 in the V-band when using a glint 10^3 times (7.5 magnitudes) brighter than the satellite to assist fringe tracking for (a) a V=16 magnitude satellite, (b) a V=14 magnitude satellite, and (c) a V=12 magnitude satellite. The solid curves are for MROI and the dashed for NPOI. At MROI, to obtain ten resolution elements takes 1 month, several days, one day for V=16, 14, and 12 respectively. At NPOI the corresponding integration times are many years, a few years, and one year, respectively.

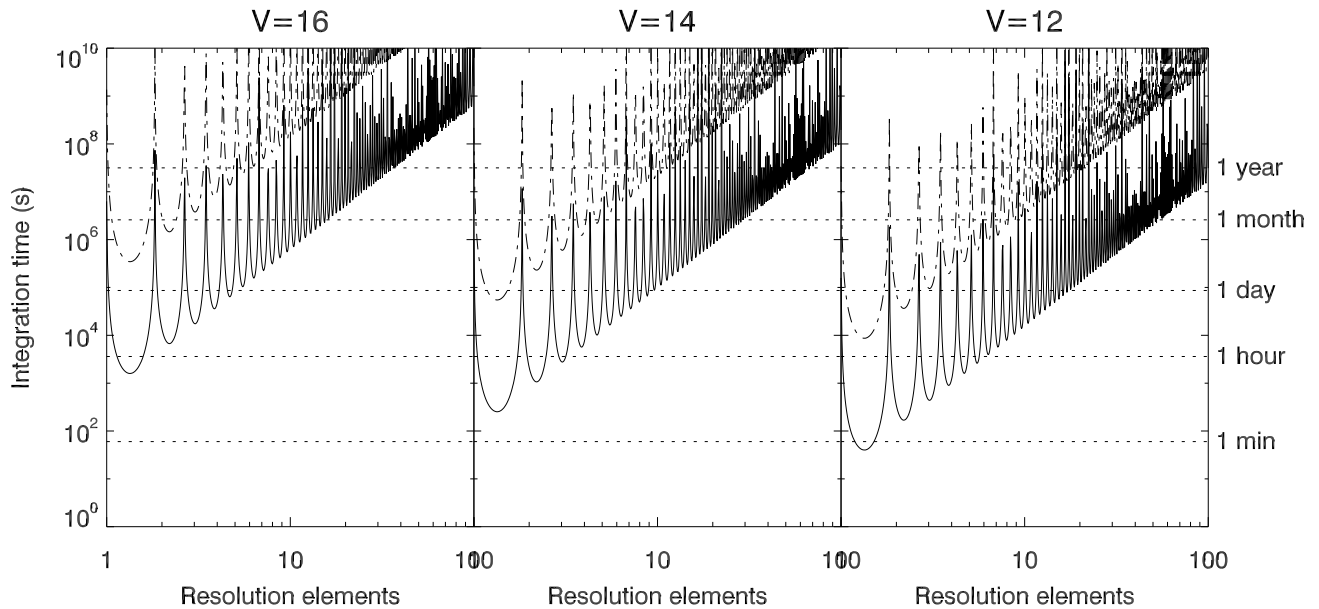


Figure 12. Integration time required to obtain imaging SNR of 10 in the H-band when using a glint 10^3 times (7.5 magnitudes) brighter than the satellite to assist fringe tracking for (a) a V=16 magnitude satellite, (b) a V=14 magnitude satellite, and (c) a V=12 magnitude satellite. The solid curves are for MROI and the dashed for NPOI. At MROI, to obtain ten resolution elements takes several days, one day, and several hours for V=16, 14, and 12 respectively. At NPOI the corresponding integration times are several years, one year, and several months, respectively.

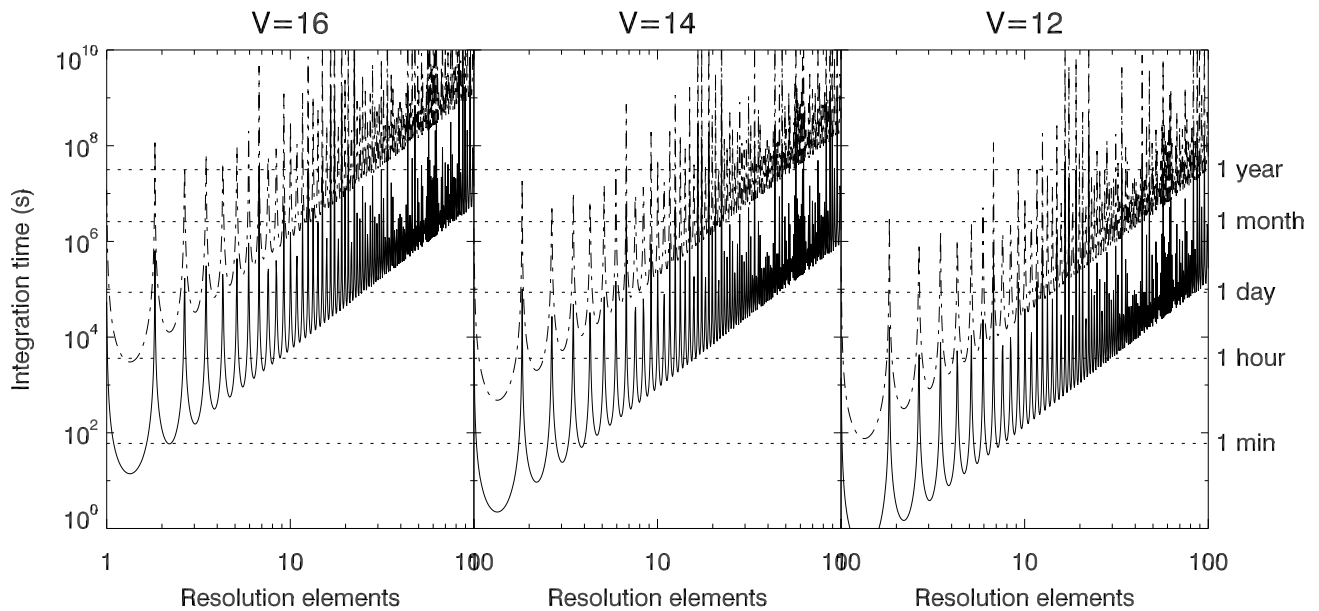


Figure 13. Integration time required to obtain imaging SNR of 10 in the V-band when there is no glint present for (a) a V=16 magnitude satellite, (b) a V=14 magnitude satellite, and (c) a V=12 magnitude satellited. The solid curves are for MROI and the dashed for NPOI. At MROI, to obtain ten resolution elements takes one hour, many minutes, and few minutes, for V=16, 14, and 12 respectively. At NPOI the corresponding integration times are nearly one month, a few days, and one day, respectively.

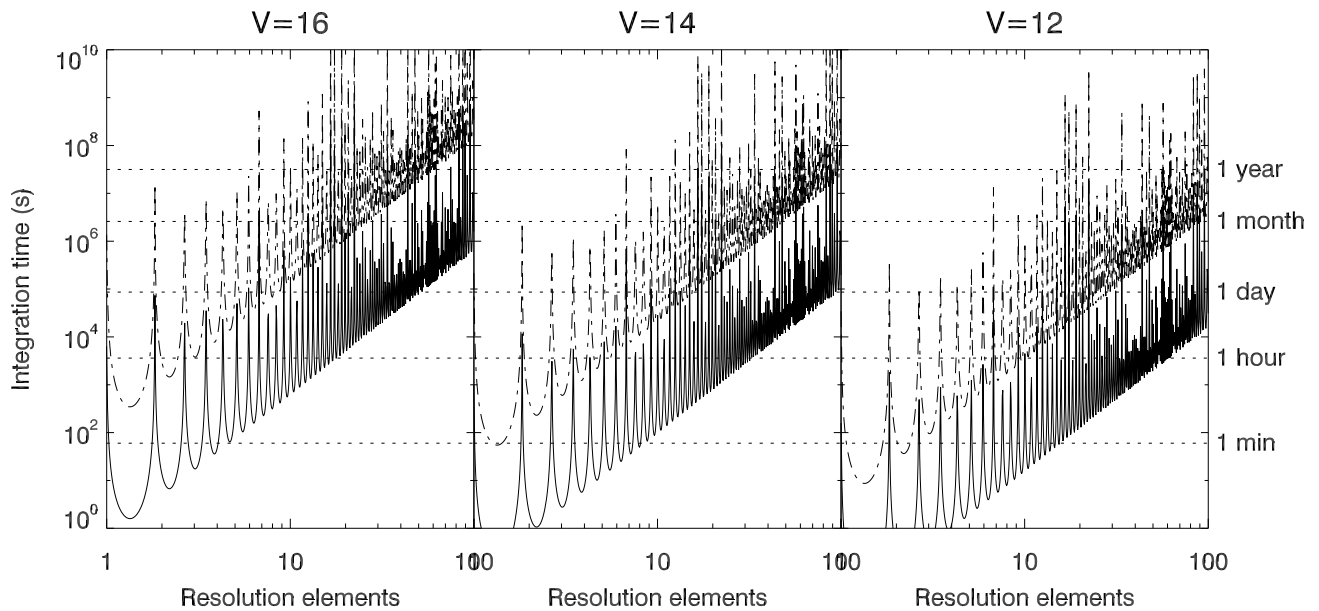


Figure 14. Integration time required to obtain imaging SNR of 10 in the H-band when there is no glint present for (a) a V=16 magnitude satellite, (b) a V=14 magnitude satellite, and (c) a V=12 magnitude satellited. The solid curves are for MROI and the dashed for NPOI. At MROI, to obtain ten resolution elements takes several minutes, about one minute, and less than one minute for V=16, 14, and 12 respectively. At NPOI the corresponding integration times are two days, several hours, and approximately one hour, respectively.

is in-fact a serious problem at the MROI site. Analysis of seeing measurements (G. Loos, unpublished report) suggests that the observatory will perform below specifications at least 98% of the time. The effect is that the fringe-tracking performance will not be as good as computed in Figure 10 and that the integration time will be longer than that computed in Figures 11-14. Whether this will affect the observatory's ability to image geostationary satellites remains to be seen.

A glint, such as occurs approximately twice per year near equinox, will make fringe-tracking much simpler. However, we also found that imaging while tracking fringes on a glint actually decreases imaging performance dramatically. The reason is that increasing the satellite brightness by a certain factor, α , by introducing the glint will effectively reduce the visibilities by that factor as well. In order to recover the SNR on the visibilities the integration time must be increased by a factor α^2 . This is not helpful because the glint only occurs for a few minutes for a few days twice a year. The glint time could be increased either by placing a emitting beacon on the satellite or placing a mirror on the satellite which can be directed to reflect light in the direction of the observatory. However these methods cannot be used on existing satellites or on satellites belonging to uncooperative organizations. And, none of this eliminates the need to integrate α^2 times longer.

A possible alternative is to illuminate the entire satellite. Increasing the illumination from the ground by shining a beacon uniformly across the satellite would increase the photon rate without reducing the visibilities of the satellite. It is thus potentially a means of improving the fringe tracking and shortening the integration time. However, if we imagine increasing the illumination of the satellite by a factor of 10, thus reducing the integration time by that much, we will be illuminating the satellite at 10 kW/m^2 , which may well be beyond the safe operating mode of the satellite. In addition, the power required from the ground is substantial. Illuminating a beam of diameter 100 m at 10 kW/m^2 will require a total power output approaching 100 MW. Further, to allow fringe-tracking and coherent integration (which is necessary), this power cannot be at a single wavelength but must be distributed across a range of wavelengths.

Another alternative is to use large apertures with adaptive optics. We have already shown that apertures of the size of those of MROI should be able to both track fringes and obtain imaging SNR in a reasonable amount of time if the apertures are phased, as is assumed in the computations in this paper. However, at

most astronomical sites, phasing an aperture of that size to its diffraction limit will require adaptive optics. The next step is then to determine the effectiveness with which an adaptive optics system can phase a large aperture on 12th to 16th V magnitude satellites.

8. CONCLUSION

We have found that to obtain a resolution at geostationary orbit of approximately one meter requires aperture diameters of the order of a hundred meters or more. It is currently unrealistic to expect single telescopes of those sizes. To obtain that resolution we therefore resort to interferometric techniques. To obtain interferometric images requires a sufficiently large number of baselines, a large enough photon rate on short baselines to track fringes, and sufficiently long integration time to obtain the necessary imaging SNR to produce images. By employing wavelength synthesis it is possible to obtain a sufficiently large number of baselines, in 10-elements interferometer, to be able to produce crude images. Fringe-tracking is possible with large apertures of similar size to those at the MROI, on the shortest baselines in H-band. However, any deviation from ideal conditions, be they non-perfect seeing or a satellite which does not behave as a perfect reflector, can narrow the fringe-tracking window significantly. A glint can improve the fringe tracking by providing a compact bright source. However, including a glint also results in, effectively, reducing the visibilities of the satellite, thereby requiring longer integration time to obtain sufficient SNR. For realistic glint brightnesses the increase in the required integration time is so large that it becomes practically impossible to image the satellite behind a glint. Using large apertures, such as those at the MROI, enough photons are collected to obtain the necessary SNR in a reasonable amount of time, if the individual telescopes are operating at the diffraction limit. At the MROI site this is rarely the case. However, if a suitable adaptive optics system can be implemented which allows diffraction limited operation to $V=13$ or $H=10$, we expect MROI to be able to make at least crude images of a number of geostationary satellites. Similar upgrades can also be made at NPOI. With larger apertures, which are planned, and adaptive optics it is also reasonable to expect NPOI to be able to make crude images of some geostationary satellites.

However, in order to definitively determine the viability of geostationary satellite imaging with an optical interferometer it is necessary to model the systems and measurement processes more realistically than the crude assumptions made in this paper. In particular, a

more realistic satellite model than the spherical diffuse reflector is needed, a better model of the fringe-tracking system, the seeing, adaptive optics, detectors, and atmospheric absorption are needed.

ACKNOWLEDGMENTS

The NPOI is funded by the Office of Naval Research and the Oceanographer of the Navy. The MRO is funded by the US Navy. This work was supported by the National Science Foundation under grant AST-0909184. This work was also supported by New Mexico Institute of Mining and Technology.

REFERENCES

1. J. T. Armstrong, D. Mozurkewich, L. J. Rickard, D. J. Hutter, J. A. Benson, P. F. Bowers, N. M. E. II, C. A. Hummel, K. J. Johnston, D. F. Buscher, J. H. C. III, L. Ha, L.-C. Ling, N. M. White, and R. S. Simon, "The navy prototype optical interferometer," The Astrophysical Journal **496**, pp. 550–571, 1998.
2. J. T. Armstrong, R. B. Hindsley, S. R. Restaino, J. A. Benson, D. J. Hutter, F. J. Vrba, R. T. Zavala, S. A. Gregory, and H. R. Schmitt, "Observations of a geosynchronous satellite with optical interferometry," in Proc. Advanced Maui Optical and Space Surveillance Technologies Conference, 2009.
3. J. T. Armstrong, R. B. Hindsley, S. R. Restaino, J. A. Benson, D. J. Hutter, F. J. Vrba, R. T. Zavala, S. A. Gregory, and H. R. Schmitt, "Observations of geosynchronous satellite with optical interferometry," in Proc. Adaptive Coded Aperture Imaging, Non-imaging, and Unconventional Imaging Sensor Systems, S. Rogers, D. P. Casasent, J. J. Dolne, T. J. Karr, and V. L. Gamiz, eds., p. 74680K, 2009.
4. J. T. Armstrong, R. B. Hindsley, S. R. Restaino, R. T. Zavala, J. A. Benson, F. J. Vrba, D. J. Hutter, S. A. Gregory, H. R. Schmitt, J. R. Andrews, and C. C. Wilcox, "Observations of a geosynchronous satellite with optical interferometry," in Adaptive Coded Aperture Imaging, Non-Imaging, and Unconventional Imaging Sensor Systems II, S. Rogers, D. P. Casasent, J. J. Dolne, T. J. Karr, and V. L. Gamiz, eds., p. 78180L, 2010.
5. J. T. Armstrong, R. B. Hindsley, H. R. Schmitt, F. J. Vrba, J. A. Benson, D. J. Hutter, and R. T. Zavala, "Detection of a geostationary satellite with the Navy Prototype Optical Interferometer," in Proc. Optical and Infrared Interferometry II, W. C. Danchi, F. Delplancke, and J. K. Rajagopal, eds., pp. 77343C–77343C–7, 2010.
6. V. J. Gamiz, R. B. Holmes, S. R. Czysak, and D. G. Voelz, "GLINT: program overview and potential science objectives," in Proc. SPIE 4091, Imaging Technology and Telescopes, J. W. Bilbro, J. B. Breckinridge, R. A. Carreras, S. R. Czyzak, M. J. Eckart, R. D. Fiete, and P. S. Idell, eds., pp. 304–315, 2000.
7. D. J. Sanchez, S. A. Gregory, D. K. Werling, T. E. Payne, L. Kann, L. G. Finkner, D. M. Payne, and C. K. Davis, "Photometric measurements of deep space satellites," in Proc. SPIE 4091, Imaging Technology and Telescopes, J. W. Bilbro, J. B. Breckinridge, R. A. Carreras, S. R. Czyzak, M. J. Eckart, R. D. Fiete, and P. S. Idell, eds., 2000.
8. T. E. Payne, S. A. Gregory, and K. Luu, "Ssa analysis of geos photometric signature classifications and solar panel offsets," in Proc. Advanced Maui Optical and Space Surveillance Technologies Conference, 2006.
9. E. J. Bakker, D. A. Klinglesmith, A. M. Jorgensen, D. Westpfahl, V. Romero, and C. Cormier, "Imaging of geostationary satellites with the mro interferometer," in Proc. Advanced Maui Optical and Space Surveillance Technologies Conference, 2009.
10. W. Cotton, J. Monnier, F. Barron, K.-H. Hofmann, S. Kraus, G. Weigelt, S. Rengaswamy, E. Thiebaut, P. Lawson, W. Jaffe, C. Hummel, T. Pauls, H. Schmitt, P. Tuthill, and J. Young, "2008 imaging beauty contest," in Proc. SPIE optical and infrared interferometry, M. Schöller, W. C. Danchi, and F. Delplancke, eds., **7013**, pp. 70131N–70131N–14, 2008.
11. D. F. Buscher, "Direct maximum-entropy image reconstruction from the bispectrum, very high angular resolution imaging," in Proc. 158th IAU symposium, 1994.
12. A. M. Jorgensen, D. Mozurkewich, T. Armstrong, H. Schmitt, C. Gilbreath, R. Hindsley, and T. A. Pauls, "Improved coherent integration through fringe model fitting," Astronomical Journal **134**, pp. 1544–1550, 2007.